Electronic Supplementary Material (ESI) for EES Catalysis.

Supporting Information

Reducing the pH dependence of Hydrogen Evolution Kinetics via Surface Reactivity Diversity in Medium-Entropy Alloys

*Bao Zhang**+, Jia Yao+, Jia Liu, Tao Zhang, Houzhao Wan*, Hao Wang*

Experimental Section

Density functional theory calculation (DFT) Calculations. The DFT calculations[1,2] are performed by using Vienna Ab-initio Simulation Package (VASP)[3] with Projector Augmented Wave (PAW) method[4] and PBE functional[5,6]. The kinetic energy cutoff of plane-waves is 500 eV. The geometry optimizations are performed by using the conjugated gradient method, and the convergence threshold is set to be 10^{-4} eV in energy and 0.05 eV $Å^{-1}$ in force. A vacuum layer of 15 Å is applied for all calculated models. The Brillouin zone is sampled by using the Monkhorst−Pack scheme[7].

The free energy of water adsorption is defined as:

$$G_{H_2O^*} = G_{sur-H_2O} - G_{H_2O} - G_{sur}$$

where $G_{sur-H2O}$, G_{H2O}, and G_{sur} are the free energies of water adsorbed, water species and clean surfaces, respectively. The free energy of hydrogen adsorption is defined as:

$$G_{H^*} = G_{sur-H} - \frac{1}{2}G_{H_2} - G_{sur}$$

where G_{sur-H}, G_{H2}, and G_{sur} are the free energies of hydrogen adsorbed, hydrogen gas and clean surfaces, respectively. The free energy diagrams were calculated using the equation:

$$G = E + ZPE - TS$$

where *G, E, ZPE* and *TS* are the free energy, total energy from DFT calculations, zero point energy and entropic contributions (T was set to be 300K), respectively. *ZPE* could be derived after frequency calculation by:

$$ZPE = \frac{1}{2}\sum h\nu_i$$

The *TS* values of adsorbed species are calculated after obtaining the vibrational frequencies[8]:

$$TS_\nu = k_B T\left[\sum_K \ln\left(\frac{1}{1-e^{-h\nu/k_B T}}\right) + \sum_K \frac{h\nu}{k_B T}\frac{1}{(e^{h\nu/k_B T}-1)} + 1\right]$$

The *d* band center can be calculated average the *d* band of surface metal:

$$\varepsilon_d = \frac{\int_{-\infty}^{E_f} x\rho(x)\,dx}{\int_{-\infty}^{E_f} \rho(x)\,dx}$$

For evaluating the water dissociation energy barrier, the transitional state is located using the Nudged Elastic Band method.[9] The Fermi softness was calculated by using Zhuanglin's methode[10]. The grand canonical potential (GCP) calculations was calculated by Goddard III's

methode[11].

Synthesis of Ni alloys on iron foam (IF). First, a piece of IF was sonicated in 1.0 M HCl for 10 min to remove the oxides layer on the top surface, then washed with ethanol and deionized water, respectively, and dried in air. The Ni alloys were electrodeposited by hydrogen bubble dynamic template. Typically, 10 mmol $NiSO_4 \cdot 6H_2O$ and 15mmol $Na_3C_6H_5O_7 \cdot 2H_2O$, 2 mmol $CuSO_4 \cdot 5H_2O$ and 1 mmol $Na_2MoO_4 \cdot 2H_2O$ were dissolved in 50 mL deionized water. After gentle stirring for 30 min, the solution was then transferred to 100 mL homemade electrolytic cell with iron foam as working electrode and Pt electrode as counter electrode with a distance of about 0.5 cm. The NiCuMo electrode (0.5 cm * 1 cm) was deposited at high current of -3 A cm^2 for 5 min on DC power supply. Finally, the product was taken out, rinsed with deionized water and ethanol several times and dried at 60 °C in air. And the loading of NiCuMo alloy is about 14.4 mg/cm^2.

Materials Characterization. The morphology and the structure of the electrodes were characterized by a field emission scanning electron microscopy (SEM; Gemini SEM 300). TEM images were obtained from JEM 2100F. Powder X-ray diffraction (XRD) patterns were acquired on a Philips X'Pert PRO with Cu Kα radiation, λ = 1.5418Å. The X-ray photoelectron spectroscopy (XPS) spectra were measured on Kratos AXIS Ultra DLD-600W XPS system equipped with a monochromatic Al K (1486.6 eV) as X-ray source. XAS data were collected at 1W1B station in Beijing Synchrotron Radiation Facility using Si (111) monochromator in transmission mode. Raman measurements were performed on inVia Reflex Raman spectrometer with a 532 nm wavelength incident laser.

Electrochemical Measurements. All the electrochemical measurements were conducted using a CHI760E potentiostat (CH Instruments, China) in a typical three electrode setup, with a piece of freshly-made electrode as the working electrode, a carbon rod as the counter electrode and an Ag/AgCl electrode as the reference electrode. Electrochemical impedance spectroscopy was

conducted at an overpotential of 100 mV with an amplitude of 10 mV. The distribution of relaxation times (DRT) analysis was performed by using DRTtools with Gaussian-basis function discretization method[12].The alkaline HER activity was also evaluated by a Hg/HgO reference electrode. Prior to every measurement, a resistance test was made and the iR compensation was applied to all initial data for further analysis. LSV measurements were conducted at a scan rate of 2 mV s^{-1} at room temperature. All polarization curves were iR-corrected unless noted. All the potentials were calibrated with respect to a RHE by the equation E(RHE) = E(Ag/AgCl) + 0.198 V + 0.059*pH and E(RHE) = E(Hg/HgO) + 0.114 V + 0.059*pH. EIS measurements were carried out in the frequency range of 100 kHz–0.1Hz at potential of 150 mV versus RHE. The electrochemical surface areas (ECSA) can be calculated by:

$$ECSA = \frac{C_{\mathrm{edl}}(\mathrm{mF cm^{-2}})}{40\ \mu F * \mathrm{cm^{-2}}\ per\ cm^2_{ECSA}}$$

The alkaline water electrolyzer was comprised of the NiCoFe layered triple hydroxide anode (electrode size of 2.0 cm^2), NiCuMo cathode (electrode size of 1.0 cm^2), gas diffusion layer, and anion exchange membrane (FAA-3-50, Fumasep). nickel foam and carbon paper were employed as the anodic and cathodic gas diffusion layers in alkaline electrolyzer, respectively. A commercial Pt/C powder with a Nafion binder (10 wt%) was used as the cathode and coated on carbon paper with a loading of 0.3 mg_{Pt} cm^{-2}. The neutral water electrolyzer was comprised of the IrO_2 anode (electrode size of 2.0 cm^2), NiCuMo cathode (electrode size of 1.0 cm^2), Ti felt gas diffusion layer, and proton exchange membrane (Nafion 117). The IrO_2 anode was comprised of 1.5 mg cm^{-2} IrO_2 and 20 wt% Nafion binder. The water electrolysis cell was operated with an electrolyte of 1 M KOH or pure water at a rate of 30 mL/min. The electrolyzer measurements were performed with a Zahner electrochemical workstation. The polarization curves were recorded at a scan rate of 10 mV s^{-1}.

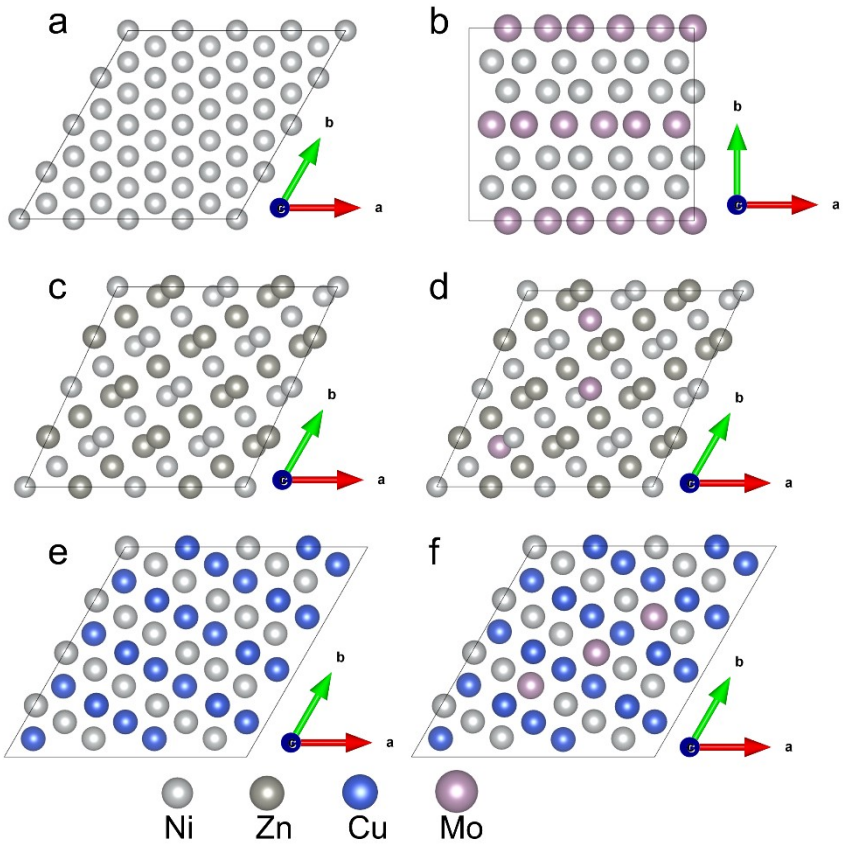

Figure S1. DFT models of (a) Ni, (b) NiMo, (c) NiZn, (d) NiZnMo, (e) NiCu, and (f) NiCuMo, respectively. Atomic color representation: light grey ball for Ni, dark grey ball for Zn, blue ball for O, and purple-grey ball for Mo.

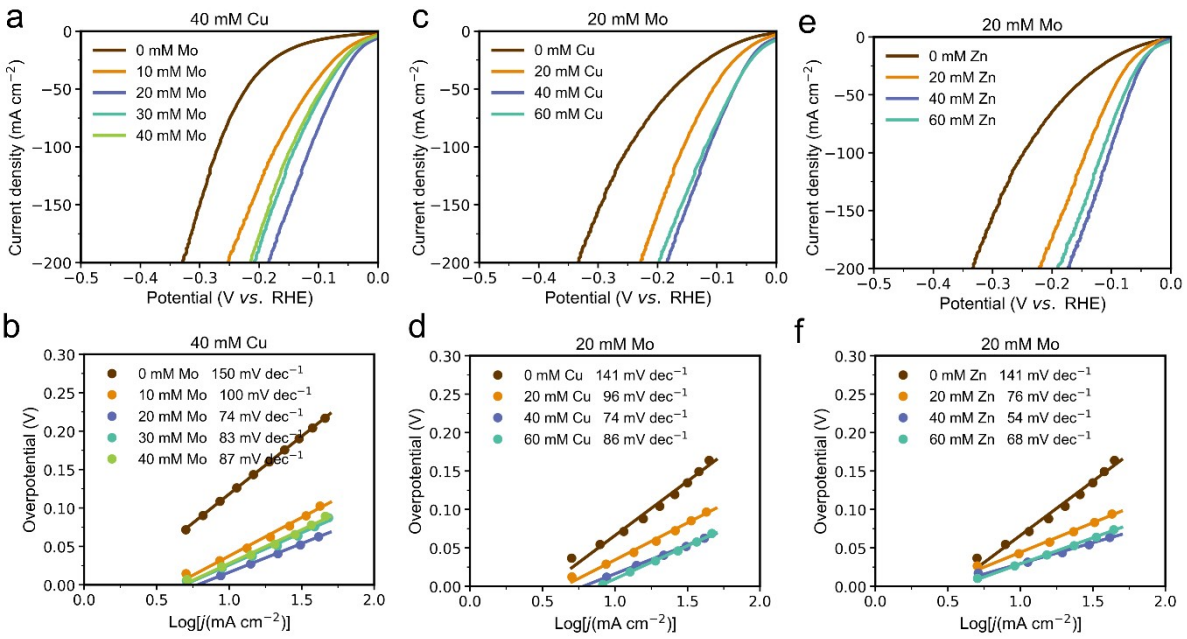

Figure S2. LSV curves of NiCuMo with various (a) Cu content and (c) Mo content. Tafel plots of NiCuMo with various (b) Mo content and (d) Cu content. (e) LSV curves and (f) Tafel plots of NiZnMo with various Mo content.

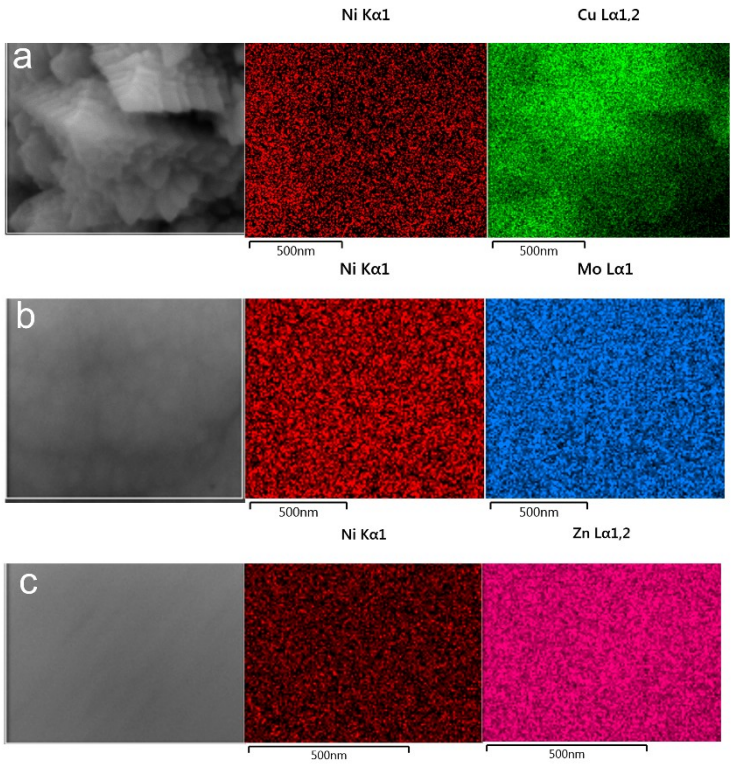

Figure S3. EDS mapping images of (a) NiCu, (b) NiMo, and (c) NiZn.

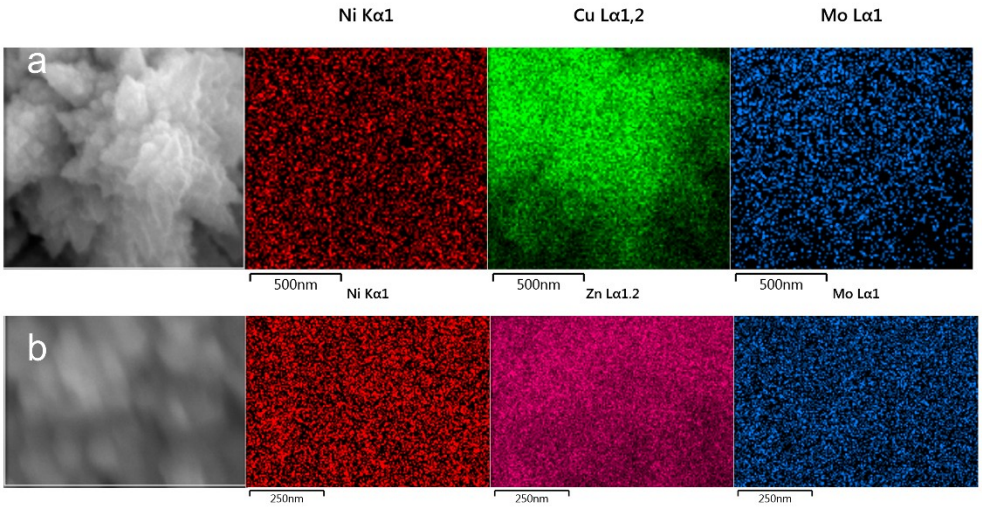

Figure S4. EDS mapping images of (a) NiCuMo and (b) NiZnMo.

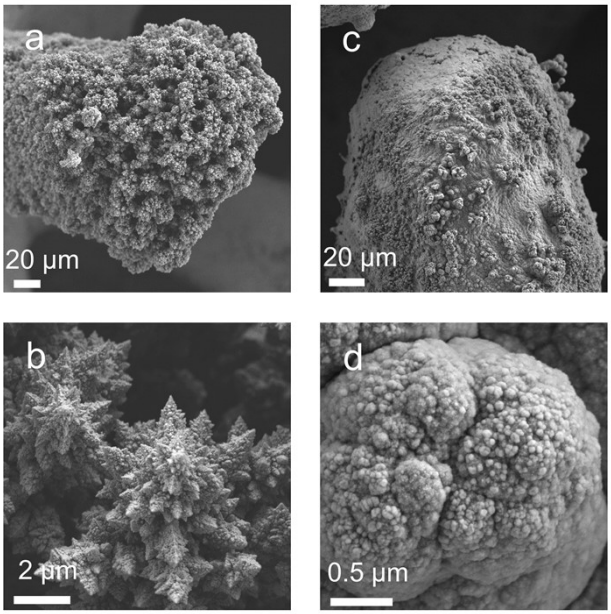

Figure S5. The SEM images of (a-b) NiCuMo and (c-d) NiZnMo.

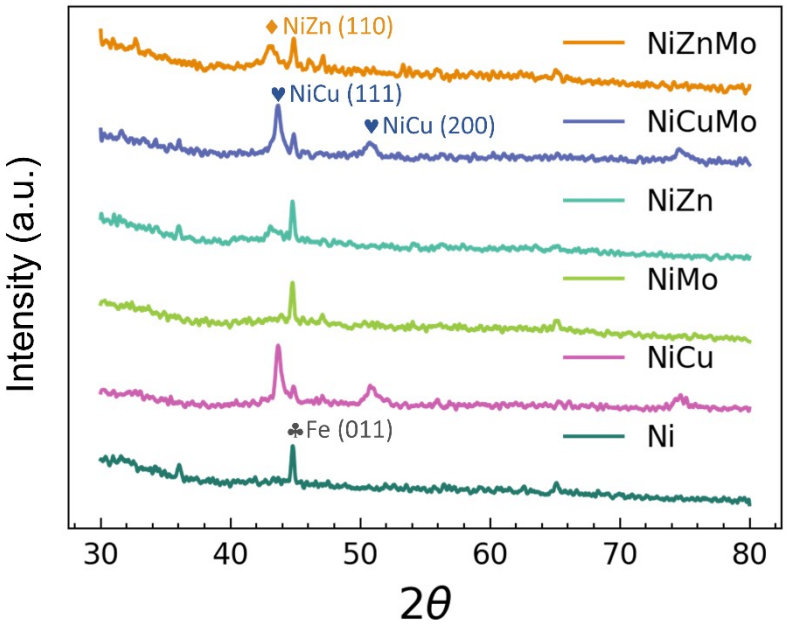

Figure S6. XRD patterns of as-prepared Ni alloy.

The typical peaks of Ni on iron foam at 44.8° can be attributed Fe (011) (PDF 96-900-6590). This is similar with NiMo alloy, which has no characteristic peaks of electrodeposited product. The typical peaks of NiCu and NiCuMo at 43.7° and 51.0° can be attributed NiCu (111) and NiCu (200) (PDF 03-065-9048). Those peaks of NiZn and NiZnMo at 43.2° can be attributed NiZn (110) (PDF 03-065-3203).

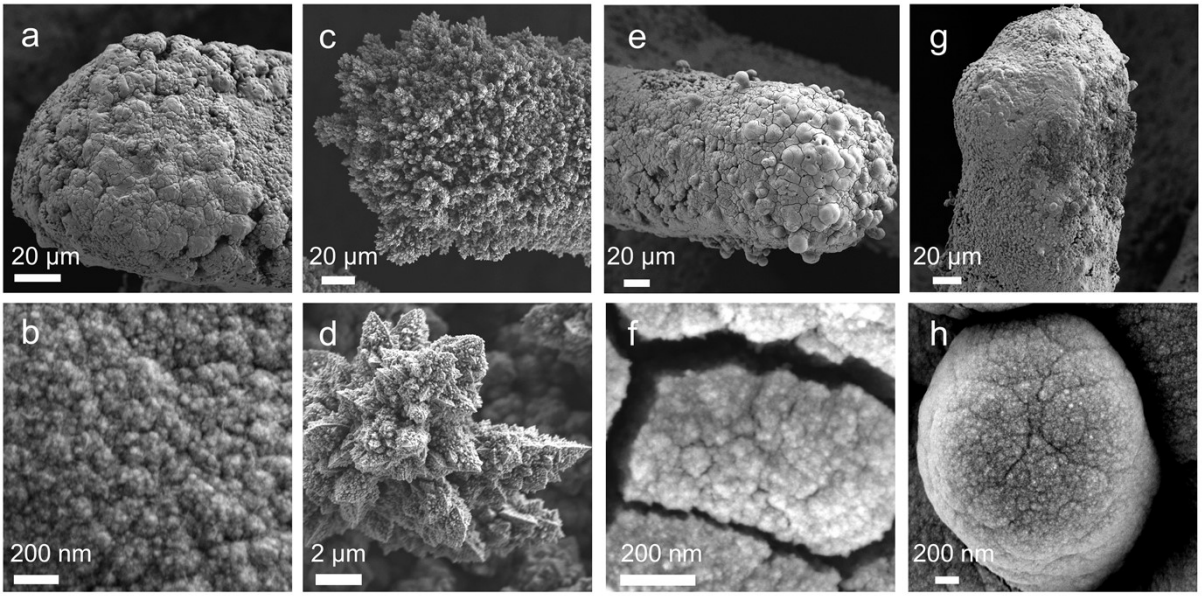

Figure S7 The SEM images of (a-b) Ni, (c-d) NiCu, (e-f) NiZn, and (g-h) NiMo.

As shown in Figure S7, the Ni sample is composed of small nanoparticles with a rougher surface. This is similar with NiMo and NiZn samples. However, NiCu sample displays a much porous structure, indicating this porous structure can be attributed to the introducing of Cu.

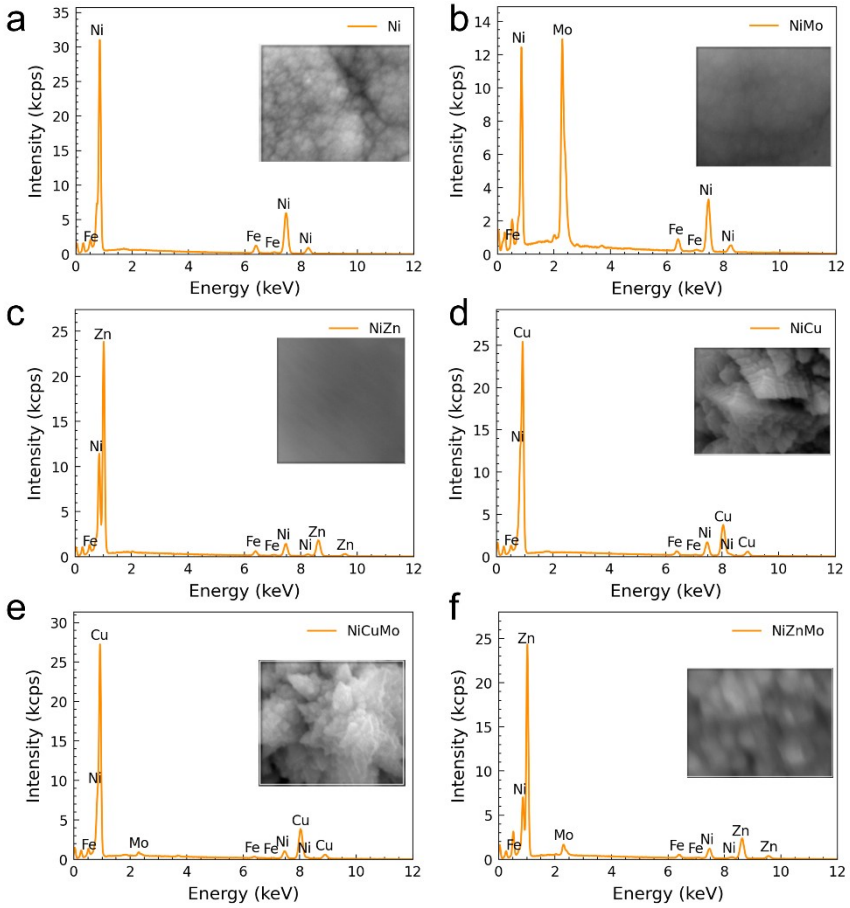

Figure S8. EDS spectra of (a) Ni, (b) NiMo, (c) NiZn, (d) NiCu, (e) NiCuMo, and (f) NiZnMo.

Table S1. Mass ratio of each metal in Ni alloy based on EDS tests.

wt%	NiCu	NiMo	NiZn	NiCuMo	NiZnMo
Ni	22.0	52.2	22.9	14.3	18.7
Cu	78.0			83.8	
Mo		47.8		1.9	5.6
Zn			77.1		75.7

Table S2. Mass ratio of each metal in NiXMo tenary alloys based on ICP-OES tests.

wt%	NiCuMo	NiZnMo
Ni	32.6	82.4
Cu/Zn	61.1	13.6
Mo	6.3	4.0

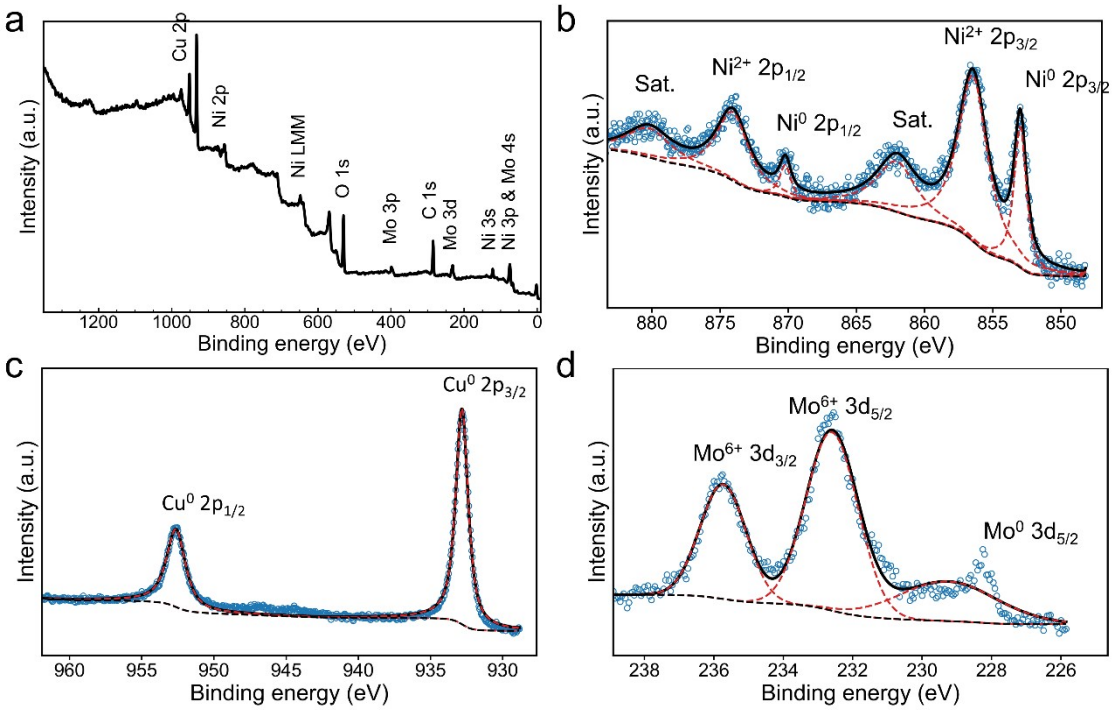

Figure S9. (a) XPS survey of NiCuMo and High-resolution XPS of (b) Ni 2p, (c) Cu 2p, and (d) Mo 3d.

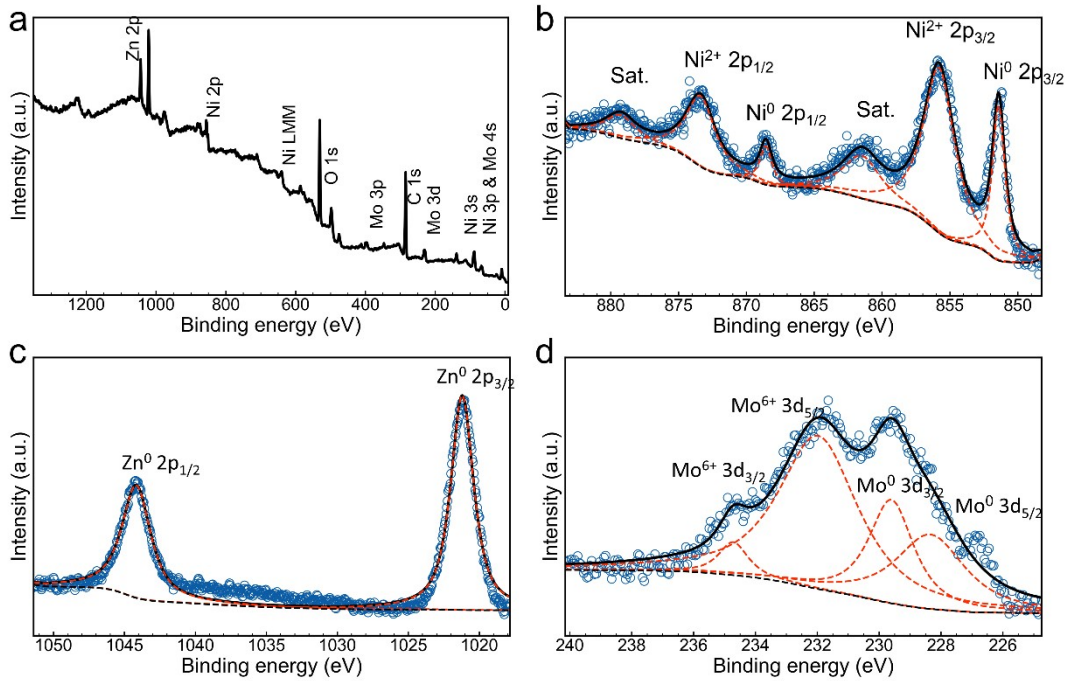

Figure S10. (a) XPS survey of NiZnMo and High-resolution XPS of (b) Ni 2p, (c) Zn 2p, and (d) Mo 3d.

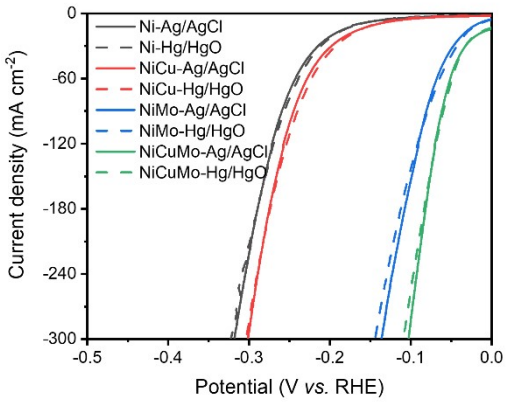

Figure S11. LSV curves of Ni-based alloys in 1M KOH with Ag/AgCl reference electrode and Hg/HgO reference electrode.

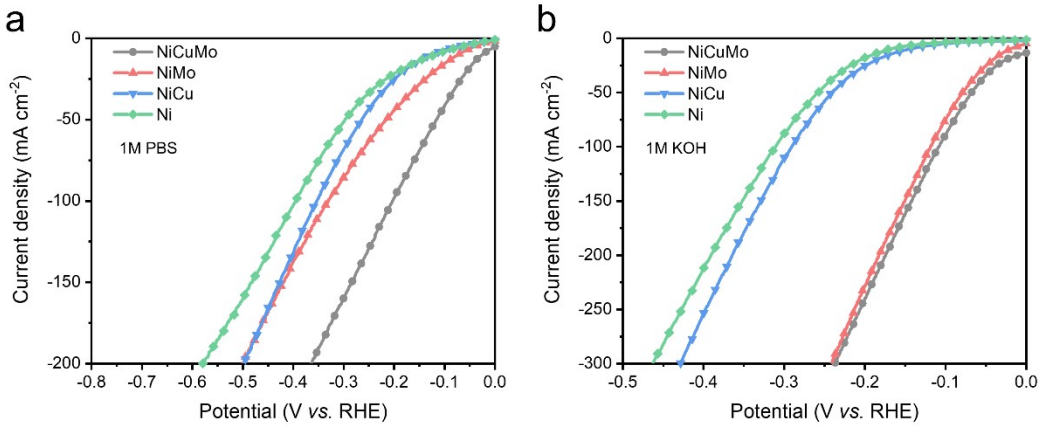

Figure S12. LSV curves of Ni-based alloys without iR correction.

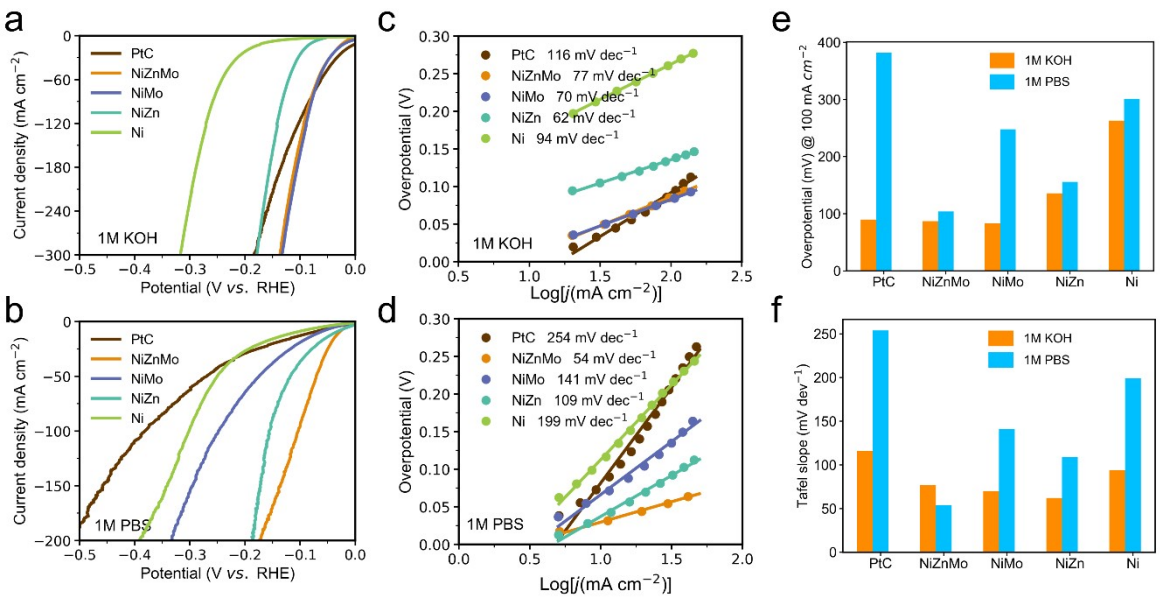

Figure S13. Linear sweep voltammetry curves of 20% Pt/C, NiZnMo, NiMo, NiZn, and Ni in (a) 1M KOH and (b) 1M PBS. Corresponding Tafel slope for various electrocatalysts in (c) 1M KOH and (d) 1M PBS. (e) Overpotentials at 100 mA cm^{-2} and (f) Tafel slopes comparison in 1M KOH and 1M PBS.

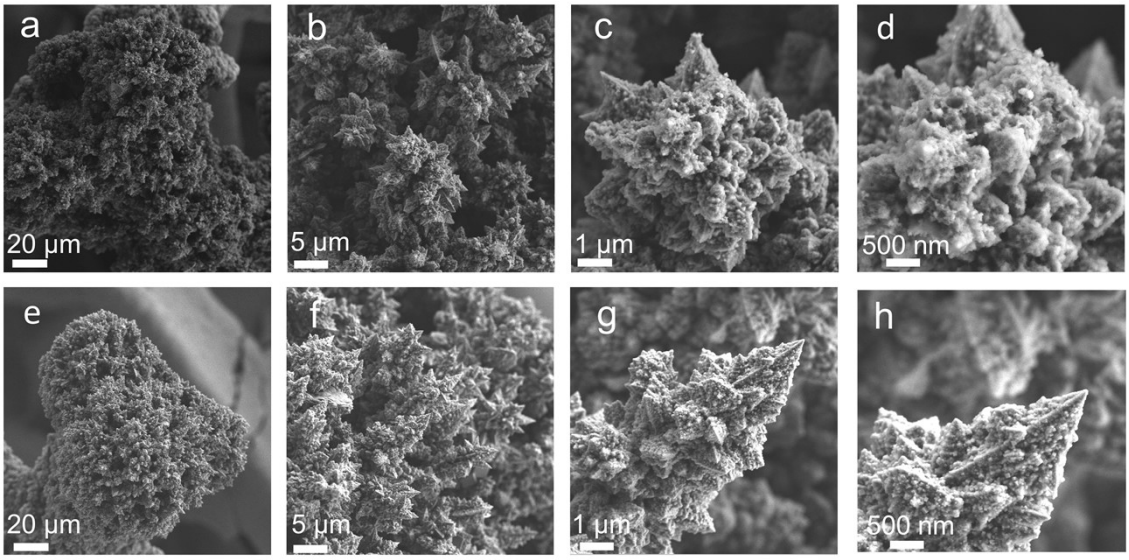

Figure S14. The SEM images of NiCuMo after long-term stability test in (a-d) 1M KOH and (e-h) 1M PBS.

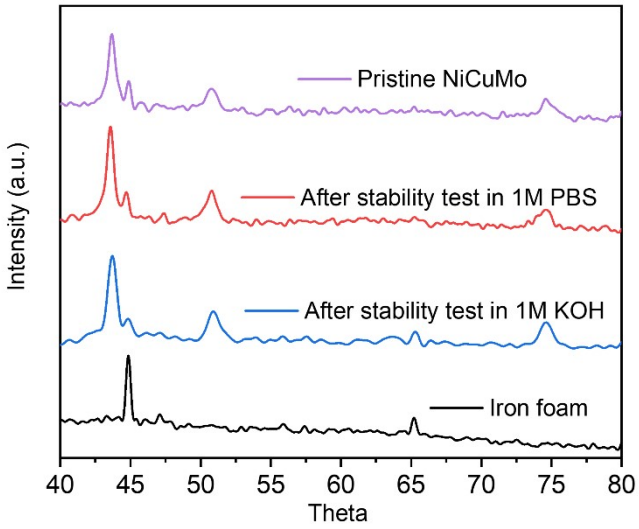

Figure S15. XRD patterns of as-prepared NiCuMo alloy and cycled alloy.

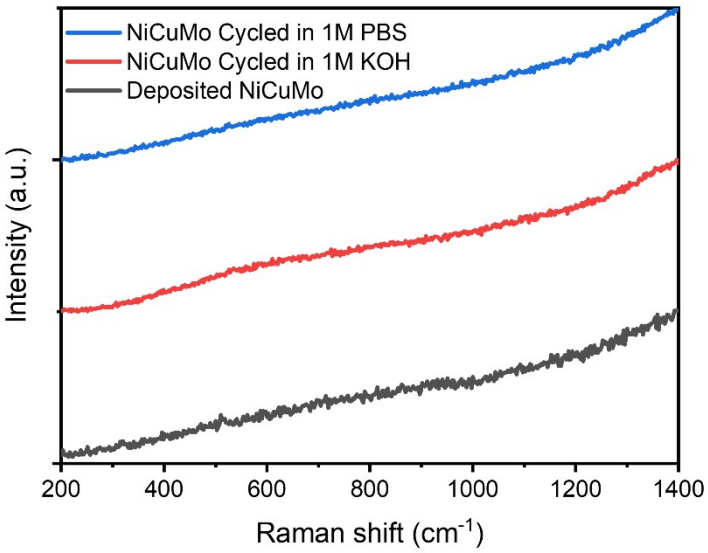

Figure S16. Raman spectra of NiCuMo after long-term stability test.

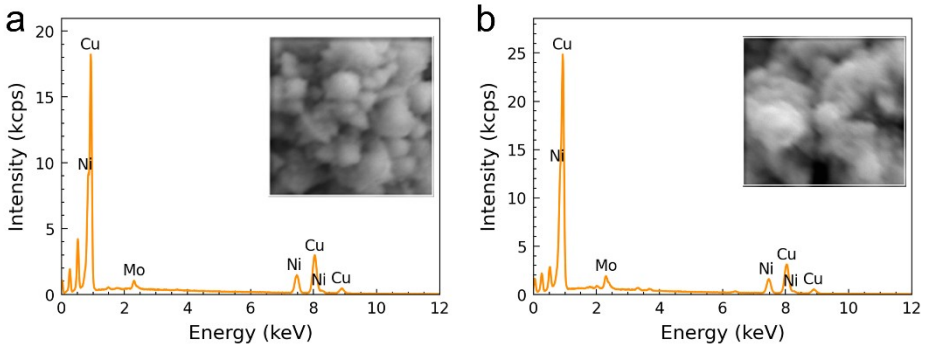

c

wt%	Initial	In 1M KOH	In 1M PBS
Ni	14.3	25.65	20.2
Cu	83.8	71.21	74.8
Mo	1.9	3.14	5.0

Figure S17. The EDS spectra of NiCuMo after stability test in (a) 1M KOH and (b) 1M PBS. (c) Corresponding metal mass ratio after stability test.

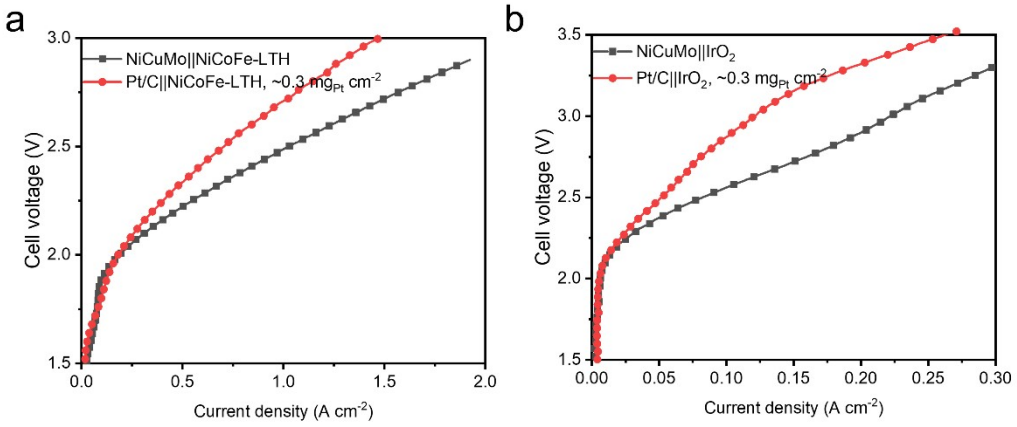

Figure S18. Membrane electrode assembly water electrolysis device performance. (a) alkaline and (b) neutral electrocatalytic water splitting performance at room temperature (20℃ ± 3℃).

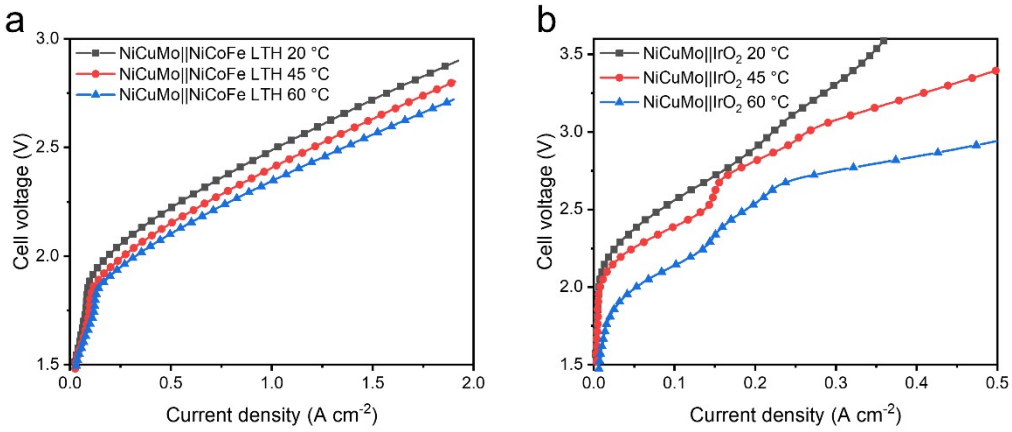

Figure S19. The polarization curves of (a) NiCuMo||NiCoFe LTH alkaline cell and(a) NiCuMo||IrO_2 neutral cell at different temperatures.

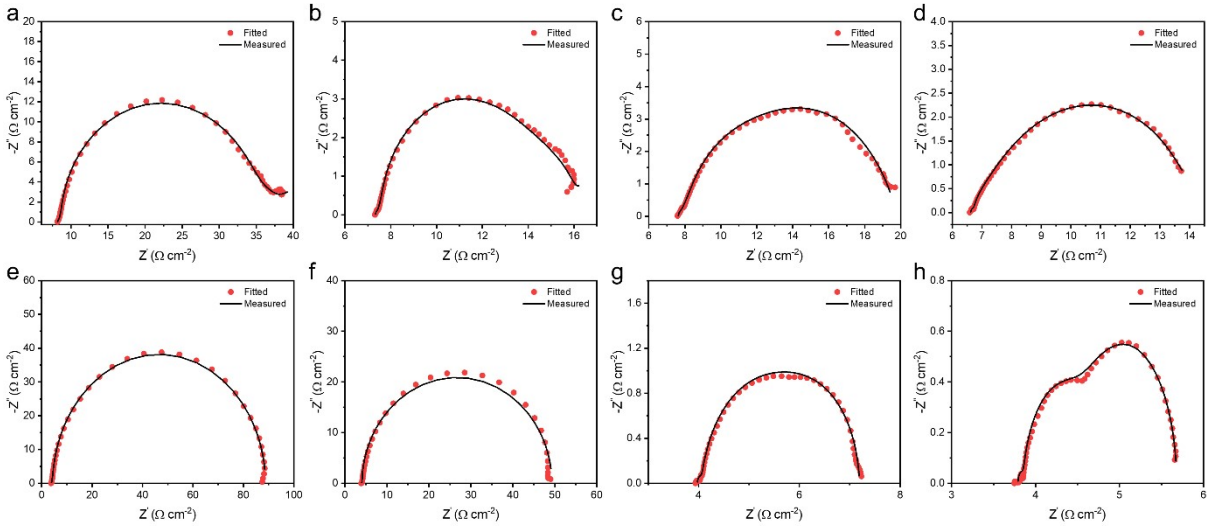

Figure S20. Electrochemical impedance spectroscopy measurements at an overpotential of 100 mV. EIS of (a)Ni, (b)NiCu, (c)NiMo, and (d)NiCuMo in 1M PBS solution. EIS data of (a)Ni, (b)NiCu, (c)NiMo, and (d)NiCuMo in 1M KOH solutions.

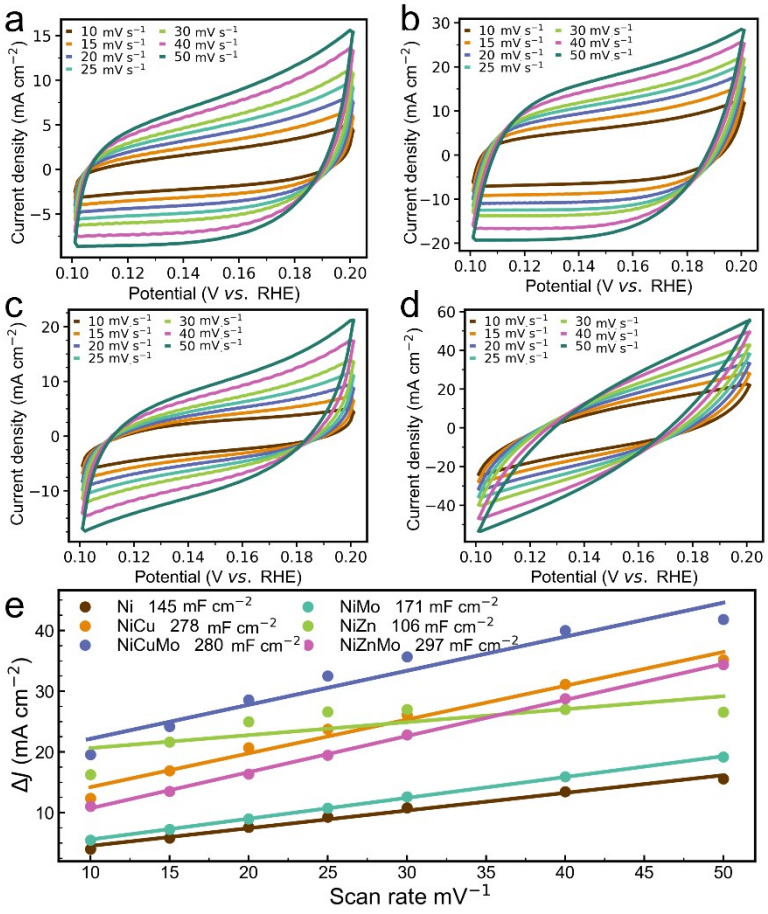

Figure S21. Cyclic voltammogram curves of (a) Ni, (b) NiCu, (c) NiMo, and (d) NiCuMo in the double layer capacitive region at the scan rates of from 10 mV/s to 50 mV/s in 1M KOH. (e) Calculated double layer capacitance.

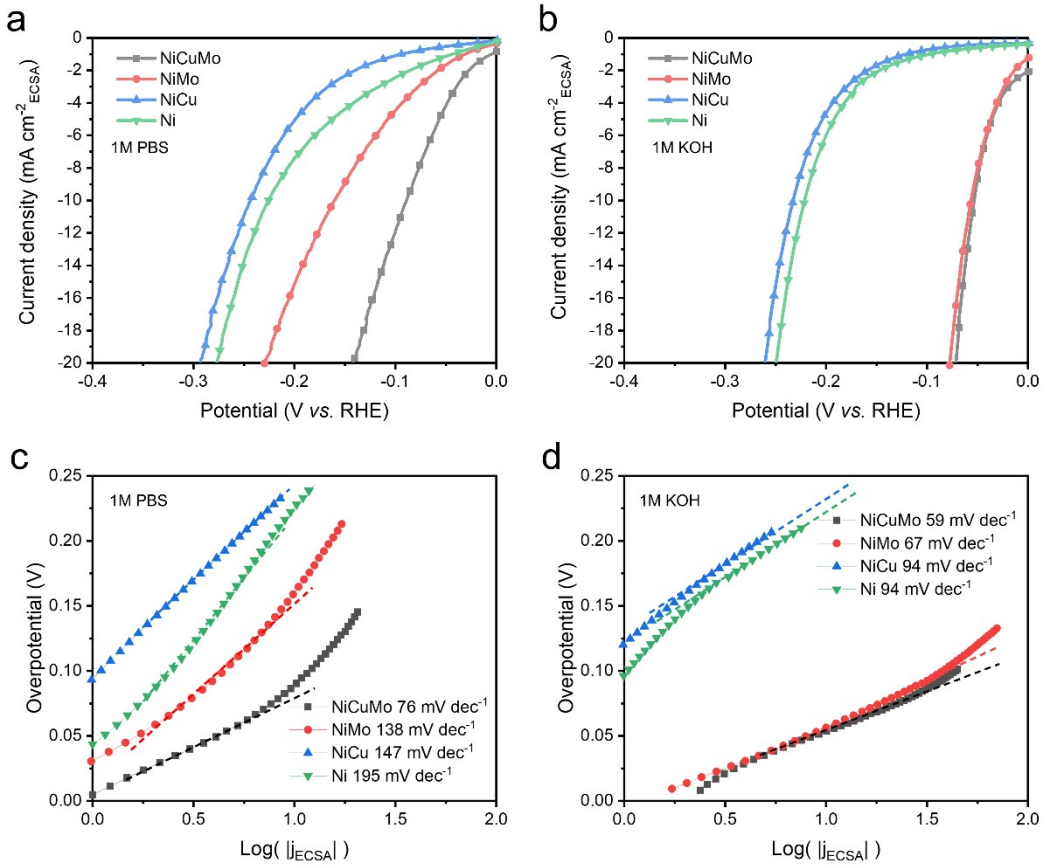

Figure S22. ECSA normalized linear sweep voltammetry curves in (a) 1M PBS and (b) 1M KOH. Corresponding Tafel slope for various electrocatalysts in (c) 1M PBS and (d) 1M KOH.

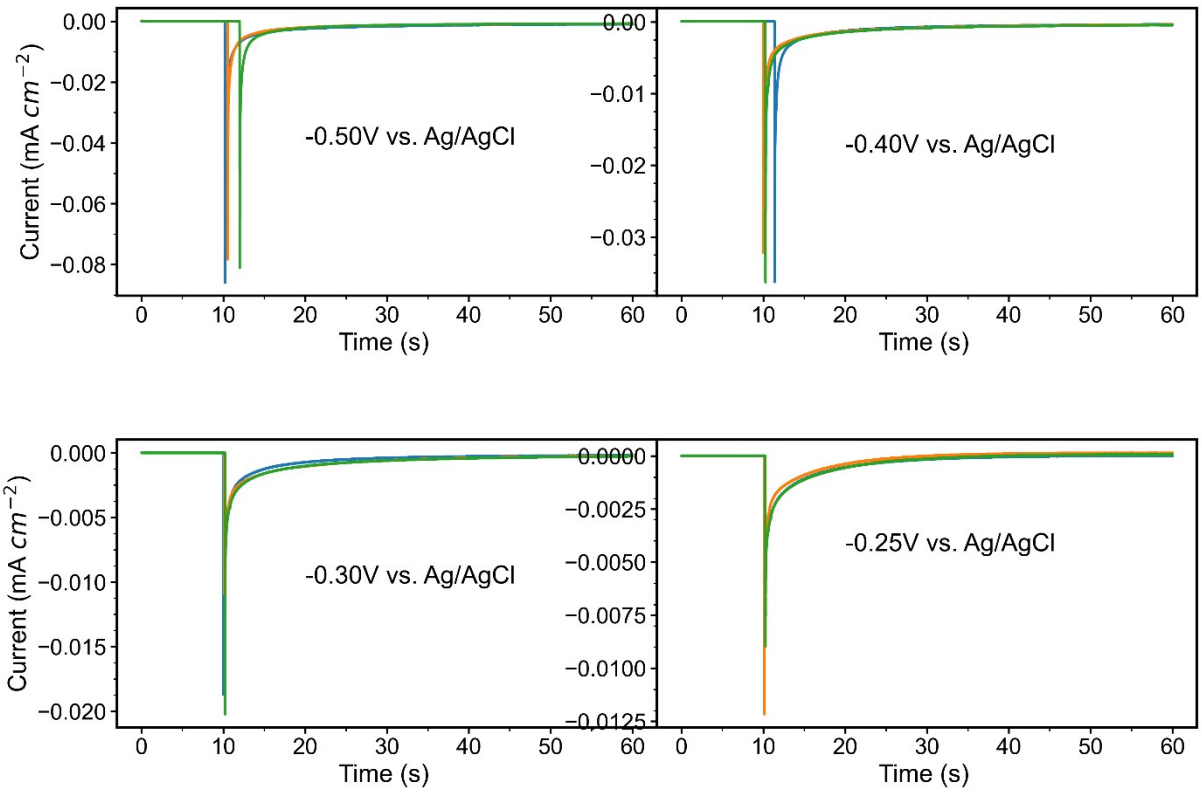

Figure S23. Current transients measured during the potentiostatic immersion of a NiCuMo electrode in 1M KOH.

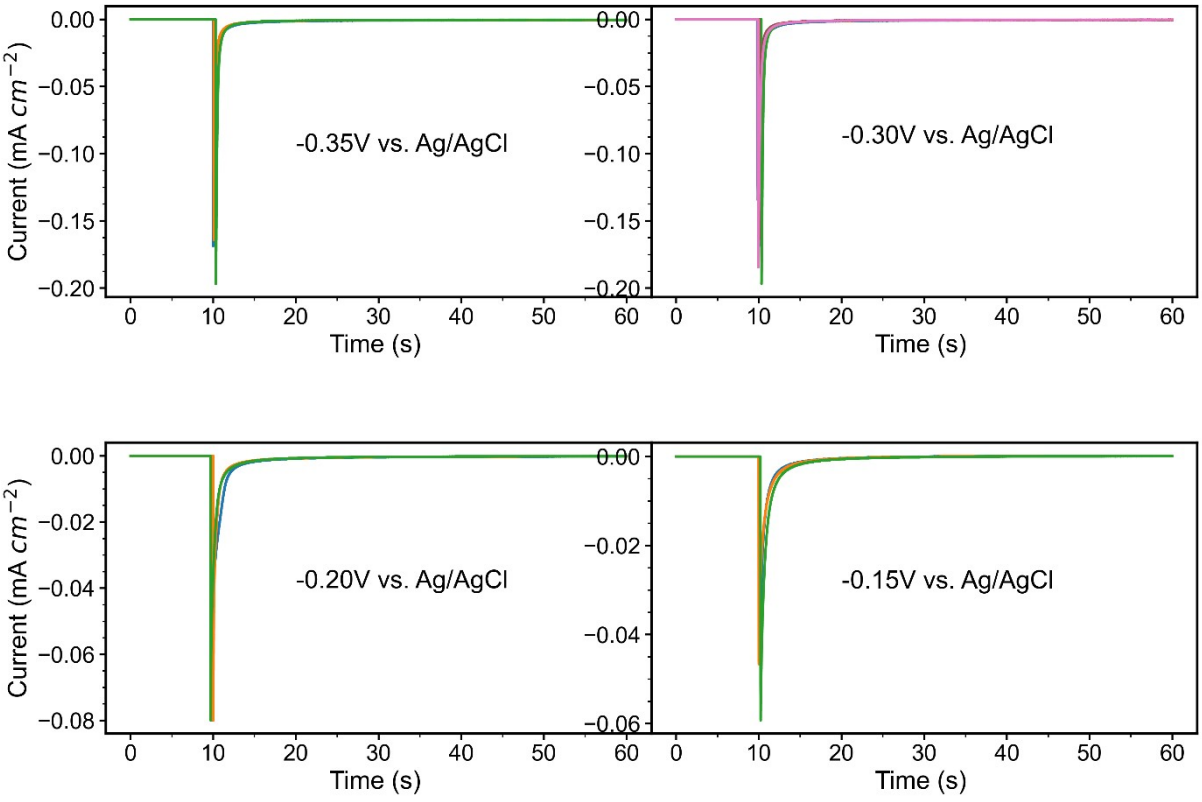

Figure S24. Current transients measured during the potentiostatic immersion of a NiCuMo

electrode in 1M PBS.

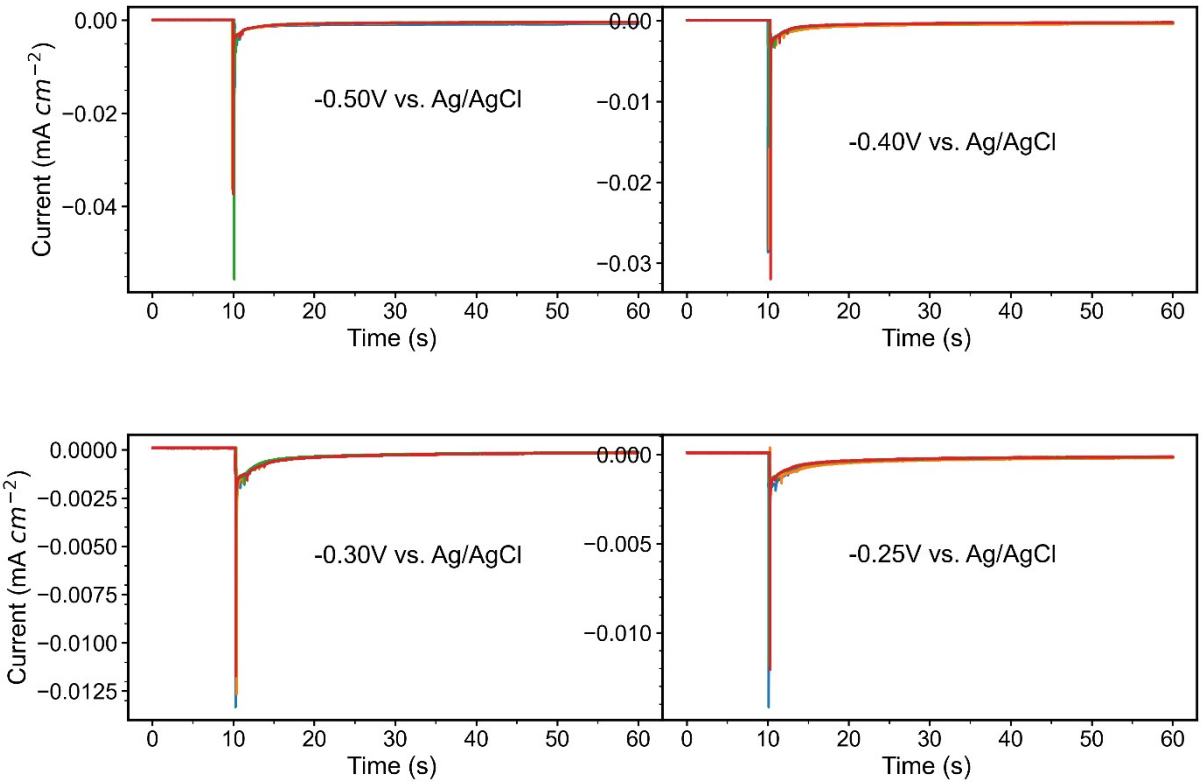

Figure S25. Current transients measured during the potentiostatic immersion of a NiMo electrode in 1M KOH.

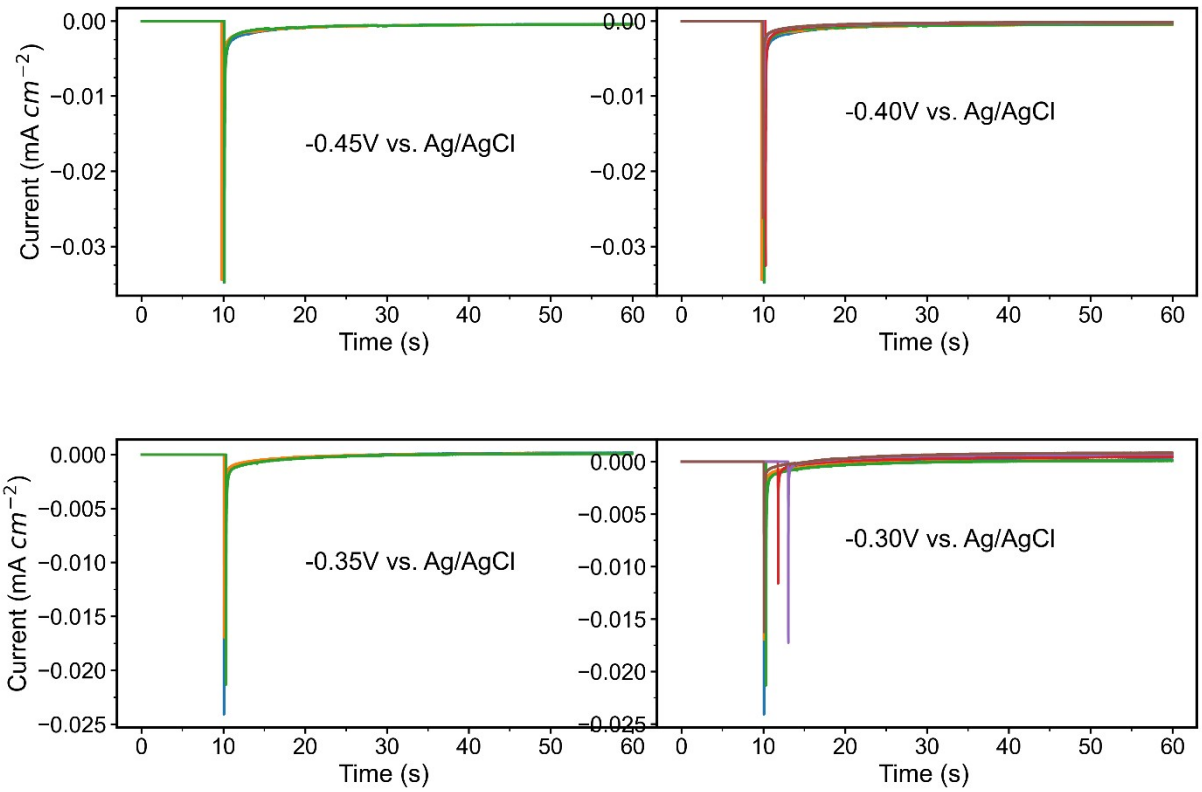

Figure S26. Current transients measured during the potentiostatic immersion of a NiMo electrode in 1M PBS.

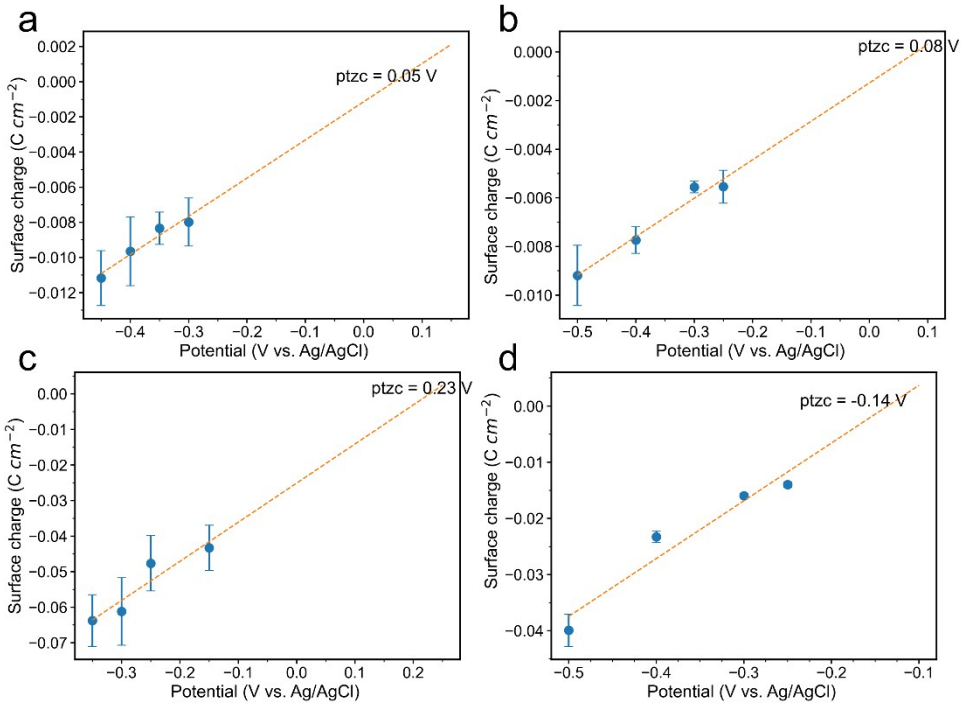

Figure S27. Integrated surface charges of (a) NiCuMo in 1M KOH, (b) NiCuMo in 1M PBS, (b) NiMo in 1M KOH and NiMo in 1M PBS.

Table S3. The alkaline HER activities of the NiCuMo and the reported electrocatalysts

Electrocatalysts	Overpotential at 100 mA cm^{-2}	Tafel slope ($mV\ dec^{-1}$)	Reference
NiCuMo	63	61	This work
Cr-Ni NH	234	72	[13]
Ni_3N_{1-x}	>100	54	[14]
NF/NiMoO-H_2	53	43	[15]
$NiCo_2P_x$	127	34	[16]
Cr-Co_4N	99	38	[17]
Co-NiS_2 NSs	>150	43	[18]
Mo-$Co_{0.85}Se$/NC	234	51	[19]
F-Ni_3S_4	92	46	[20]
$Ni(OH)_2/MoS_2$	~150	60	[21]
Mo-Ni_3N	88	64	[22]
Ni/Yb_2O_3	81	44.6	[23]
O-NiCu	69	34.1	[24]
F-Ni_3S_4	92	46.2	[25]
M-Co_3O_4	203	63	[26]
(Co,Ni)OOH-P	149	41	[27]
Ni-Co_2P	185	77.6	[28]
$NiCeWO_x$	215	91.5	[29]
$(Fe_{0.74}Co_{0.26})_2P/Ni_3N$	113	na	[30]
NiMo	~115	Na	[31]

Table S4. The neutral HER activities of the NiCuMo and the reported electrocatalysts

Electrocatalysts	Overpotential (mV)	Tafel slope ($mV\ dec^{-1}$)	Reference
NiCuMo	114 @ 100 mA cm^{-2} 71 @ 50 mA cm^{-2}	74	This work
CrO_x/Cu–Ni	~150 @ 100 mA cm^{-2}	64	[32]
Mn-Ni-S/NF	>200 @ 100 mA cm^{-2}	65	[33]
CoP/Co-MOF	>150 @ 100 mA cm^{-2}	63	[34]
$NiCo_2P_x$	173 @ 100 mA cm^{-2}	65	[16]
$Ni_{0.89}Co_{0.11}Se_2$	>200 @ 100 mA cm^{-2}	60	[35]
$CuCo_3$-P	219 @ 100 mA cm^{-2}	100	[36]
v-NiFe LDH	~160 @ 50 mA cm^{-2}	46.3	[37]
Ni-Co-Cr	198 @ 100 mA cm^{-2}	na	[38]
N,Cu-CoP/CC	148.4 @ 50 mA cm^{-2}	117.3	[39]
Ni-SP	214 @ 100 mA cm^{-2}	39	[40]
Cu-CoP NAs/CP	~155 @ 50 mA cm^{-2}	83.5	[41]
*p*Fe/FeP	260 @ 50 mA cm^{-}	66	[42]
Co-FePO/OH	198 @ 100 mA cm^{-}	72.5	[43]
Ru–Co_xP	112.7 @ 100 mA cm^{-}	52.1	[44]
CuAlNiMoFe	~180 @ 100 mA cm^{-}	50	[45]
N-CoP/CC	~150 @ 50 mA cm^{-}	69	[46]
N-Co_2P/CC	~100 @ 50 mA cm^{-}	68	[47]
np-$Co_9S_{8-x}P_x$	~170 @ 50 mA cm^{-}	51	[48]

Reference:

1 P. Hohenberg and W. Kohn, *Phys. Rev.*, 1964, **136**, B864.
2 W. Kohn and L. J. Sham, *Phys. Rev.*, 1965, **140**, A1133.
3 G. Kresse and J. Hafner, *Phys. Rev. B*, 1993, **47**, 558.
4 P. E. Blöchl, *Phys. Rev. B*, 1994, **50**, 17953.
5 G. Kresse and J. Furthmüller, *Phys. Rev. B*, 1996, **54**, 11169.
6 J. P. Perdew, K. Burke and M. Ernzerhof, *Phys. Rev. Lett.*, 1996, **77**, 3865.
7 H. J. Monkhorst and J. D. Pack, *Phys. Rev. B*, 1976, **13**, 5188.
8 L. I. Bendavid and E. A. Carter, *J. Phys. Chem. C*, 2013, **117**, 26048–26059.
9 G. Henkelman and H. Jónsson, *J. Chem. Phys.*, 2000, **113**, 9978–9985.
10 B. Huang, L. Xiao, J. Lu and L. Zhuang, *Angew. Chem.*, 2016, **128**, 6347–6351.
11 Y. Huang, R. J. Nielsen and W. A. I. Goddard, *J. Am. Chem. Soc.*, 2018, **140**, 16773–16782.
12 T. H. Wan, M. Saccoccio, C. Chen and F. Ciucci, *Electrochimica Acta*, 2015, **184**, 483–499.
13 J. Kim, H. Jung, S.-M. Jung, J. Hwang, D. Y. Kim, N. Lee, K.-S. Kim, H. Kwon, Y.-T. Kim, J. W. Han and J. K. Kim, *J. Am. Chem. Soc.*, 2021, **143**, 1399–1408.
14 B. Liu, B. He, H.-Q. Peng, Y. Zhao, J. Cheng, J. Xia, J. Shen, T.-W. Ng, X. Meng, C.-S. Lee and W. Zhang, *Adv. Sci.*, , DOI:10.1002/advs.201800406.
15 Z.-Y. Yu, C.-C. Lang, M.-R. Gao, Y. Chen, Q.-Q. Fu, Y. Duan and S.-H. Yu, *Energy Environ. Sci.*, 2018, **11**, 1890–1897.
16 R. Zhang, X. Wang, S. Yu, T. Wen, X. Zhu, F. Yang, X. Sun, X. Wang and W. Hu, *Adv. Mater.*, 2017, **29**, 1605502.
17 N. Yao, P. Li, Z. Zhou, Y. Zhao, G. Cheng, S. Chen and W. Luo, *Adv. Energy Mater.*, 2019, **9**, 1902449.
18 J. Yin, J. Jin, H. Zhang, M. Lu, Y. Peng, B. Huang, P. Xi and C.-H. Yan, *Angew. Chem.*, 2019, **131**, 18849–18855.
19 Q. Dai, L. Wang, K. Wang, X. Sang, Z. Li, B. Yang, J. Chen, L. Lei, L. Dai and Y. Hou, *Adv. Funct. Mater.*, 2022, **32**, 2109556.
20 J. Wang, Z. Zhang, H. Song, B. Zhang, J. Liu, X. Shai and L. Miao, *Adv. Funct. Mater.*, 2021, **31**, 2008578.
21 B. Zhang, J. Liu, J. Wang, Y. Ruan, X. Ji, K. Xu, C. Chen, H. Wan, L. Miao and J. Jiang, *Nano Energy*, 2017, **37**, 74–80.
22 B. Zhang, J. Wang, J. Liu, L. Zhang, H. Wan, L. Miao and J. Jiang, *ACS Catal.*, 2019, **9**, 9332–9338.
23 H. Sun, Z. Yan, C. Tian, C. Li, X. Feng, R. Huang, Y. Lan, J. Chen, C.-P. Li, Z. Zhang and M. Du, *nature.com.remotexs.ntu.edu.sgmunications*, 2022, **13**, 1–13.
24 J. Wang, S. Xin, Y. Xiao, Z. Zhang, Z. Li, W. Zhang, C. Li, R. Bao, J. Peng, J. Yi and S. Chou, *Angew. Chem. Int. Ed.*, 2022, **61**, e202202518.
25 J. Wang, Z. Zhang, H. Song, B. Zhang, J. Liu, X. Shai and L. Miao, *Adv. Funct. Mater.*, 2021, **31**, 2008578.
26 H. Zhang, J. Zhang, Y. Li, H. Jiang, H. Jiang and C. Li, *J. Mater. Chem. A*, 2019, **7**, 13506–13510.
27 L. Zhang, Z. Wang, J. Zhang, Z. Lin, Q. Zhang, W. Zhong and G. Wu, *Nano Res.*, 2023, 1–8.
28 J. Li, D. Chu, D. R. Baker, A. Leff, P. Zheng and R. Jiang, *ACS Appl. Energy Mater.*, 2021, **4**, 9969–9981.
29 K. Chen, R. Rajendiran, C. Deviprasath, S. Mathew, Y.-R. Cho, K. Prabakar and O. Lun Li, *ChemElectroChem*, 2022, **9**, e202200093.
30 W. Ma, D. Li, L. Liao, H. Zhou, F. Zhang, X. Zhou, Y. Mo and F. Yu, *Small*, **n/a**, 2207082.

31 F. Qin, Z. Zhao, M. K. Alam, Y. Ni, F. Robles-Hernandez, L. Yu, S. Chen, Z. Ren, Z. Wang and J. Bao, *ACS Energy Lett.*, 2018, **3**, 546–554.
32 C.-T. Dinh, A. Jain, F. P. G. de Arquer, P. De Luna, J. Li, N. Wang, X. Zheng, J. Cai, B. Z. Gregory, O. Voznyy, B. Zhang, M. Liu, D. Sinton, E. J. Crumlin and E. H. Sargent, *Nat. Energy*, 2019, **4**, 107–114.
33 L. Zeng, Z. Liu, K. Sun, Y. Chen, J. Zhao, Y. Chen, Y. Pan, Y. Lu, Y. Liu and C. Liu, *J. Mater. Chem. A*, 2019, **7**, 25628–25640.
34 T. Liu, P. Li, N. Yao, G. Cheng, S. Chen, W. Luo and Y. Yin, *Angew. Chem.*, 2019, **131**, 4727–4732.
35 B. Liu, Y.-F. Zhao, H.-Q. Peng, Z.-Y. Zhang, C.-K. Sit, M.-F. Yuen, T.-R. Zhang, C.-S. Lee and W.-J. Zhang, *Adv. Mater.*, 2017, **29**, 1606521.
36 Y. Cheng, Y. Pei, P. Zhuang, H. Chu, Y. Cao, W. Smith, P. Dong, J. Shen, M. Ye and P. M. Ajayan, *Small*, 2019, **15**, 1904681.
37 Z. Yuan, S.-M. Bak, P. Li, Y. Jia, L. Zheng, Y. Zhou, L. Bai, E. Hu, X.-Q. Yang, Z. Cai, Y. Sun and X. Sun, *ACS Energy Lett.*, 2019, **4**, 1412–1418.
38 M. J. Kenney, J. E. Huang, Y. Zhu, Y. Meng, M. Xu, G. Zhu, W.-H. Hung, Y. Kuang, M. Lin, X. Sun, W. Zhou and H. Dai, *Nano Res.*, 2019, **12**, 1431–1435.
39 H. Xu, G. Xu, L. Chen and J. Shi, *Adv. Mater.*, 2022, **34**, 2200058.
40 M. I. Abdullah, A. Hameed, N. Zhang and M. Ma, *ChemElectroChem*, 2019, **6**, 2100–2106.
41 L. Yan, B. Zhang, J. Zhu, Y. Li, P. Tsiakaras and P. Kang Shen, *Appl. Catal. B Environ.*, 2020, **265**, 118555.
42 C. Xiao, R. R. Gaddam, Y. Wu, X. Sun, Y. Liang, Y. Li and X. S. Zhao, *Chem. Eng. J.*, 2021, **408**, 127330.
43 Q. Zhang, Z. L. Zhe Ru, R. Daiyan, P. Kumar, J. Pan, X. Lu and R. Amal, *ACS Appl. Mater. Interfaces*, 2021, **13**, 53798–53809.
44 C. Wang and L. Qi, *ACS Mater. Lett.*, 2021, **3**, 1695–1701.
45 R.-Q. Yao, Y.-T. Zhou, H. Shi, W.-B. Wan, Q.-H. Zhang, L. Gu, Y.-F. Zhu, Z. Wen, X.-Y. Lang and Q. Jiang, *Adv. Funct. Mater.*, 2021, **31**, 2009613.
46 Y. Men, P. Li, F. Yang, G. Cheng, S. Chen and W. Luo, *Appl. Catal. B Environ.*, 2019, **253**, 21–27.
47 Y. Men, P. Li, J. Zhou, G. Cheng, S. Chen and W. Luo, *ACS Catal.*, 2019, **9**, 3744–3752.
48 Y. Tan, M. Luo, P. Liu, C. Cheng, J. Han, K. Watanabe and M. Chen, *ACS Appl. Mater. Interfaces*, 2019, **11**, 3880–3888.